Exp Fluids (2016) 57:112
DOI 10.1007/s00348-016-2197-6

RESEARCH ARTICLE

Characterization of zebrafish larvae suction feeding flow using μPIV and optical coherence tomography

Kerem Pekkan[1] · Brian Chang[2] · Fazil Uslu[1] · Karthick Mani[3] · Chia-Yuan Chen[3] · Roi Holzman[4,5]

Received: 21 December 2015 / Revised: 1 June 2016 / Accepted: 2 June 2016 / Published online: 16 June 2016

Abstract The hydrodynamics of suction feeding is critical for the survival of fish larvae; failure to capture food during the onset of autonomous feeding can rapidly lead to starvation and mortality. Fluid mechanics experiments that investigate the suction feeding of suspended particles are limited to adult fishes, which operate at large Reynolds numbers. This manuscript presents the first literature results in which the external velocity fields generated during suction feeding of early zebrafish larvae (2500–20,000 μm total length) are reported using time-resolved microscopic particle image velocimetry. For the larval stages studied, the maximum peak suction velocity of the inflow bolus is measured at a finite distance from the mouth tip and ranges from 1 to 8 mm/s. The average pressure gradient and the velocity profile proximal to the buccal (mouth) cavity are calculated, and two distinct trends are identified. External recirculation regions and reverse flow feeding cycles are also observed and quantified. One of the unresolved questions in fish suction feeding is the shape and dynamics of the buccal cavity during suction feeding; optical coherence tomography imaging is found to be useful for reconstructing the mouth kinematics. The projected area of the mouth cavity during the feeding cycle varies up to 160 and 22 % for the transverse and mid-sagittal planes, respectively. These findings can inspire novel hydrodynamically efficient biomedical and microfluidic devices.

1 Introduction

Larval fish experience extreme mortality rates during the first days of their lives. In the wild, over 90 % of a typical brood can perish during this "critical period." Somewhat surprisingly, larval mortality is also extremely high in mariculture facilities, where food is abundant and conditions are stable. It has recently been suggested that this mortality could be attributed to the hydrodynamic regime in which larvae dwell (China and Holzman 2014; Holzman et al. 2015; Yaniv et al. 2014). Like most aquatic vertebrates, larval fish exploit a physical reality by suction feeding to exert a hydrodynamic force on their prey. This is done by rapid expansion of the buccal cavity, which results in decreasing intra-oral pressure, thereby creating a flow of water external to the mouth. The spatiotemporal properties of the fluid flow generated due to this buccal expansion determine the efficiency of food intake (Holzman et al. 2015; Yaniv et al. 2014) and the efficiency detrimental for the survival of fish larvae (Parra and Yúfera 2000). While much is known about these patterns in juvenile and adult fishes, no direct measurements are yet available for fish larvae (reviewed in Day et al. 2015; Holzman et al. 2015).

Flow visualization and particle image velocimetry (PIV) experiments with adults from several species reveal stereotypical spatial and temporal patterns of the suction

Electronic supplementary material The online version of this article (doi:10.1007/s00348-016-2197-6) contains supplementary material, which is available to authorized users.

✉ Kerem Pekkan
kpekkan@ku.edu.tr

1 Department of Mechanical Engineering, Koç University, Rumelifeneri Yolu, Sariyer, Istanbul, Turkey

2 Department of Biomedical Engineering, Carnegie Mellon University, Pittsburgh, PA, USA

3 Department of Mechanical Engineering, National Cheng Kung University, Tainan, Taiwan

4 Department of Zoology, Tel Aviv University, Tel Aviv, Israel

5 Inter-University Institute for Marine Sciences, Eilat, Israel

flows (Day et al. 2015). Suction flows are characteristically unsteady, attaining fast flows (>3 m/s) within very short time frames (>20 ms) (Day et al. 2005; Higham et al. 2006; Holzman et al. 2008; Staab et al. 2012). Steep pressure and velocity gradients are also characteristic, with flows decaying to <1 % of their speed within a distance of one mouth (orifice) diameter (Day et al. 2005, 2007; Higham et al. 2006; Holzman et al. 2008; Staab et al. 2012). Flows typically start at the onset of mouth opening, and inward flow occurs consistently until the mouth closes. Peak flow speed is usually attained when the mouth is fully open, usually very close to the time of maximum gape. However, CFD modeling and tracking of food particles suggests that some of these patterns may change in larval fish due to the dominance of viscous forces in low Reynolds ($Re < 100$) conditions. Therefore, the present research paper experimentally investigates the low *Re* number pulsatile creeping flow performance for the larval stages of zebrafish. The development of established animal models with complete genomes, such as the zebrafish, can facilitate interdisciplinary investigations of coupled neurobiology and fluid dynamics relating to taste and smell through the use of transgenic function-controlled larvae and can help improve our understanding of the suction feeding process.

A high-speed microscopic flow visualization system equipped with time-resolved optical dissection imaging capability during the suction feeding period is necessary to elucidate the coupling effect between the rapid cranial movements and spatial synchronously induced flow fields. In this study, a new hydrodynamic approach is introduced to better address this hallmark behavior of teleost fishes.

2 Methodology

Nine individual zebrafish larvae (*Danio rerio*), belonging to three developmental groups, were used in the experiments. These subjects span early-development larvae with a total length less than 5 mm (Group 1), medium size with a total length between 5 and 10 mm (Group 2), and mature subjects with total length up to 2 cm (Group 3). A biocompatible flow tracer of mashed raw egg yolk was prepared with distilled water to reach a solution concentration of 1 %. The feeding cycle was identified by tracking the tip of the lower jaw and gill flap movements. Fish larvae were placed in a petri dish and subsequent imaging was performed dorsally, using a Leica MZ 16 FA stereomicroscope (10× magnification) with a 2× objective and a high-speed CMOS camera (Photron SA4, Photron Limited, Japan) at 1024 × 1024 image resolution for data acquisition (Supplementary Movie 1: Suction Raw Data). Image series during spontaneous feedings were typically acquired at 500 Hz, as described in an earlier publication (Chen and Pekkan 2013). Post-processing employed 32 × 32 pixel interrogation windows for the first pass and 16 × 16 for the second pass.

Optical coherence tomography (OCT) imaging was performed in a temperature and humidity controlled chamber using an interferometric technique (Kowalski et al. 2014). Acquisition was performed at 67 Hz using a spectral domain system with a 4.3-μm resolution (Ganymede, Thorlabs, Germany). The light source consisted of a super luminescent diode with a center wavelength of 930 nm. The interferogram was detected using a linear CCD array-based spectrometer. For further details of our in-house OCT system, please refer to References (Chen et al. 2013; Kowalski et al. 2014).

3 Results and discussion

3.1 Buccal cavity kinematics

The buccal volume was imaged through time-resolved OCT to provide anatomical evidence on how buccal expansion regulates suction flows. OCT allowed us to identify the active regions of the buccal volume and to distinguish between the disparate feeding and respiration cycles. Representative three-dimensional gross dimensions of the mouth cavity were measured for the zebrafish in Group 2 (see Fig. 1). We observed rapid mouth opening and closing movements associated with the feeding cycle. These movements occurred proximal to the mouth cavity, reaching a maximum 162 % increase in projected area locally, at cross sections similar to those shown in Fig. 1a. The jaw opening cycle was also verified based on the lateral movies recorded separately (see Fig. 1b). Along the mouth toward the tail, the wall motion during the feeding cycle reduced significantly, resulting in a 22 % increase in the total projected cavity area. During the suction feeding cycle, a short section of the buccal cavity, located proximal to the mouth, is observed to move significantly more than the other internal mouth regions (see Supplementary Movie 3: OCT mid-sagittal plane). This short active mouth cavity region could be associated with the reduced low Reynolds number suction performance.

One of the unresolved questions in fish suction feeding is the shape and dynamics of the buccal cavity during suction feeding, though OCT imaging has proven useful to reconstruct the 3D mouth kinematics. To our knowledge, this information has not been available in the literature for both the adult and the larval stages. Thus, the present quantitative three-dimensional imaging approach will expand upon the earlier descriptive studies of jaw kinematics, which focus entirely on the external anatomical elements

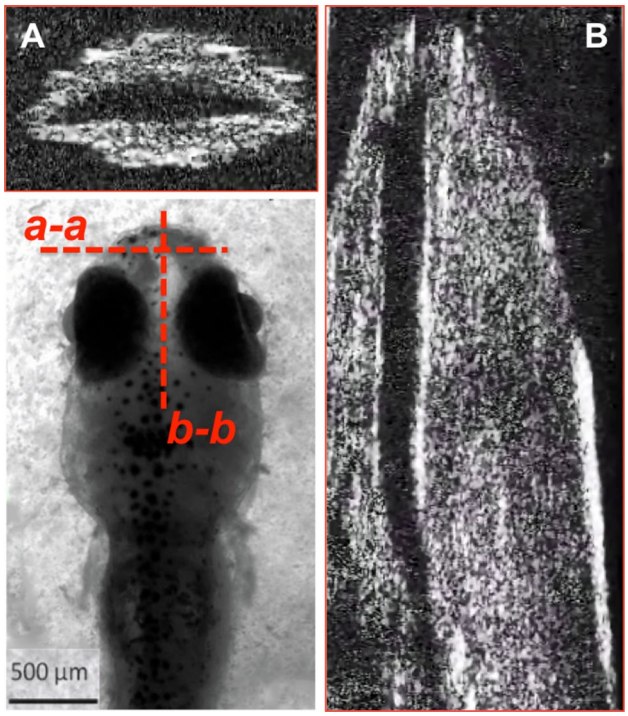

Fig. 1 Optical coherence tomography images of zebrafish larvae mouth cavity at maximum opening (see Supplementary Movie 2: OCT Transverse Plane and Supplementary Movie 3: OCT Mid-Sagittal Plane). **a** Section *a-a*, axial slice of mouth cavity. **b** Section *b-b*, anterior/posterior view of mouth cavity

using high-speed cameras (Hernandez 2000; Yaniv et al. 2014).

3.2 Flow structures

Peak inflow velocity vector fields for three representative zebrafish larvae sizes are plotted in Fig. 2. Data were recorded by viewing the top of the fish with a clear particle flow showing particles flowing both in and out of the fish. The velocity field during a typical burst event was also acquired as shown in Fig. 3 and occurred at a slightly different PIV plane than the suction. Topology of the body geometry around the mouth, in particular its symmetry or lack thereof, contributes to the three-dimensional external flow structures. This particle flow had several interesting characteristics including its symmetry and consistency, indicating that it was not necessarily flowing through the mouth. For example, we observed two symmetrical recirculation zones located symmetrically proximal to the mouth, whose strength diminished as the fish grew (see Fig. 4 for the close-up view). These external vortical structures are reported for the first time in the literature and will influence feeding performance significantly. As a result, analogous external recirculation zones can be employed in pulsatile inflow biomedical devices

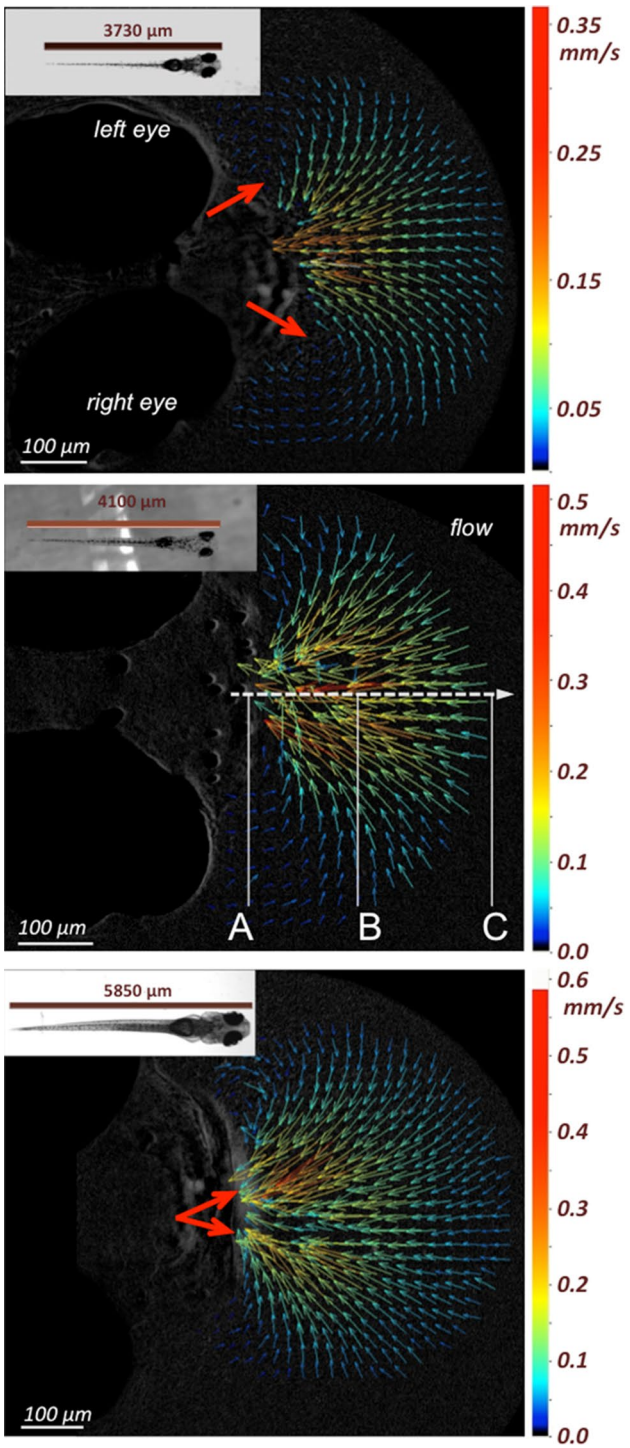

Fig. 2 Processed µPIV results showing the induced flow field by suction feeding movement of a zebrafish larva. Sample inflow velocity vector fields close to the mouth for increasing body sizes (*top* to *bottom*). µPIV measurements correspond to the frontal plane that is aligned with the mouth opening. *Inserts* show the corresponding full length of the zebrafish samples. *Arrows* refer to major flow patterns discussed in the text. The *dashed line* corresponds to the central streamline through *A*, *B*, and *C* with increasing *x*-coordinate. Pressure gradient is computed at *seven lines*, where the *central streamline* is in the middle (please see Fig. 5)

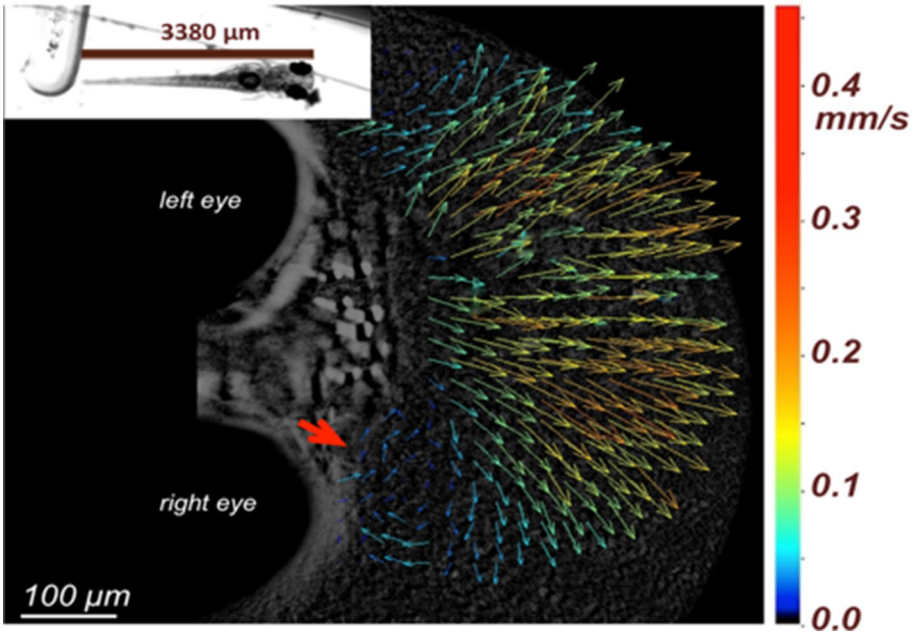

Fig. 3 Peak velocity field captured during a typical burst event for a zebrafish larva from the small size group. This outflow phenomenon occurs occasionally during feeding. *Arrow* indicates the recirculation zones generated

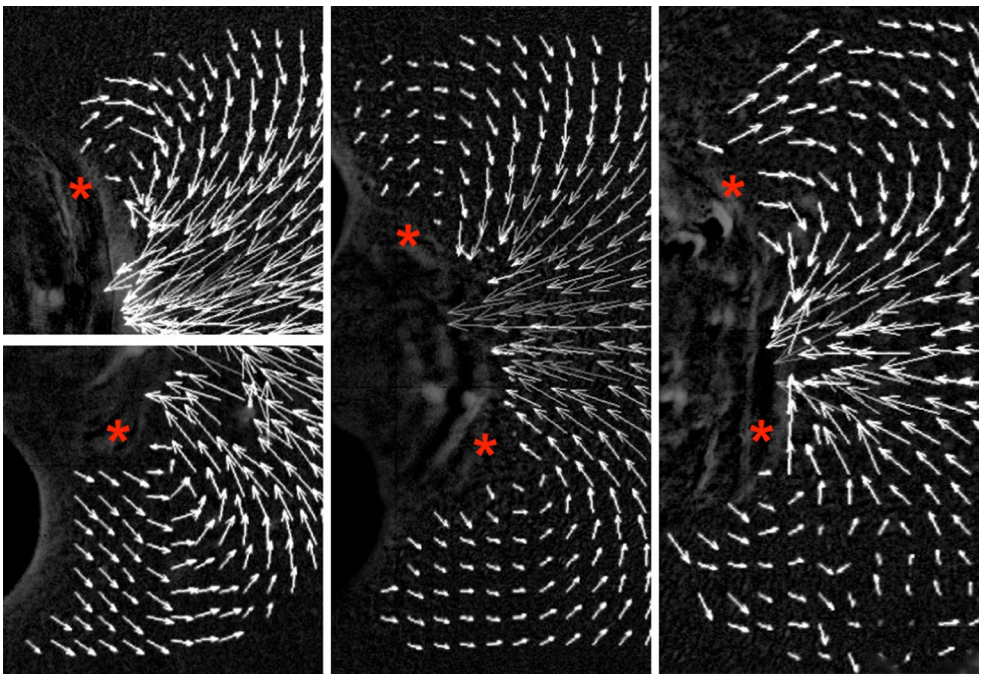

Fig. 4 Close-up views of the recirculating velocity vectors recorded from four different samples during the suction feeding cycle (marked with *asterisk*). Both symmetric as well as asymmetric recirculation zones are observed

to augment low Re internal flow; this should also prompt future studies. As the fish grew older, the inlet suction sometimes occurred through two distinct flow pathways, as shown in Fig. 2. For larger fish, higher peak velocities and longer feeding cycle periods are recorded and summarized in Fig. 5. A fully developed zebrafish larvae can extend its jaw to increase induced flow velocity to a maximum of 8 mm/s when prey is within its proximity. These measurements are in agreement with a recent tomographic PIV study of *adult* zebrafish during strike feeding, where velocity magnitudes of 45–60 mm/s are reported (Gemmell et al. 2014).

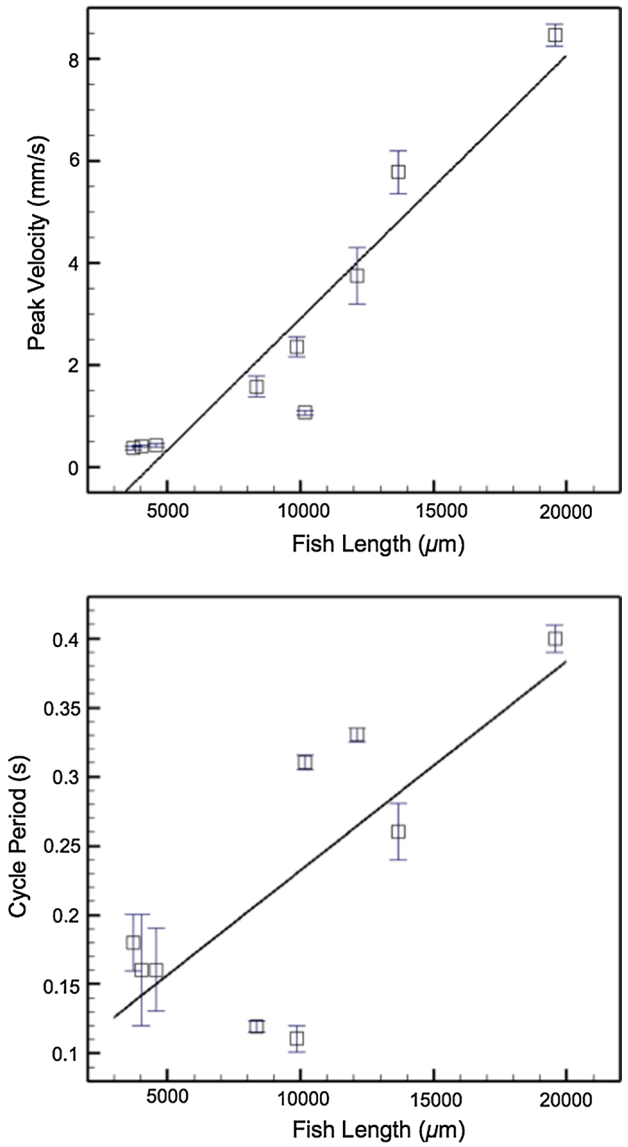

Fig. 5 Peak inflow suction velocity ($V_{peak} = -2.249 + 0.0005158L$, $R^2 = 0.90$) and feeding cycle period ($T_{feeding} = 0.08085 + 1.514e - 05*L$, $R^2 = 0.60$) for increasing zebrafish larvae size and development age. The linear regression fit for each parameter is plotted

3.3 Suction force on prey

The momentum equation along the central inflow streamline of the mouth aperture provides an estimate of the suction force during feeding, as shown in Fig. 2.

$$F_{pg} = -\frac{\mathrm{d}p}{\mathrm{d}x} L_x A_\mathrm{f}$$

L_x and A_f denote the effective length and frontal area of the prey (seeding particles), respectively. The pressure gradient can be computed from the velocity field, including two-dimensional effects (Dabiri et al. 2014);

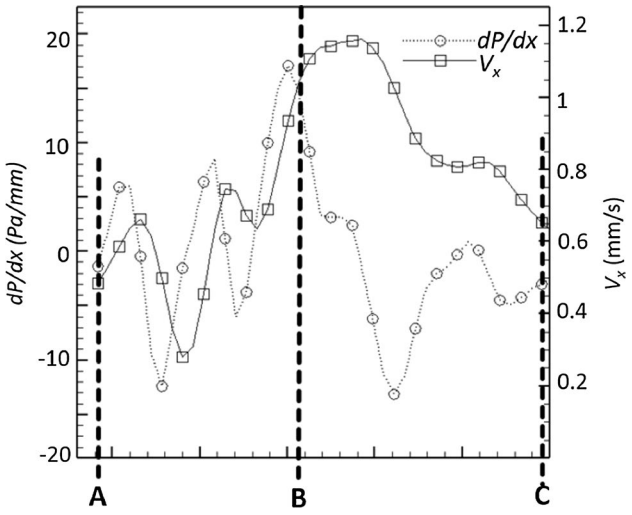

Fig. 6 Axial velocity V_x and pressure gradient dP/dx along the central inflow streamline of the zebrafish oral aperture due to induced flow field during the suction feeding. Axial velocity and pressure gradients are area-averaged around the central inflow *centerline* (shown with *dashed line* in Fig. 2). Locations of points *A*, *B*, and *C* are labeled in Fig. 2

$$\frac{\mathrm{d}p}{\mathrm{d}x} = -\rho\left(V_x\frac{\partial V_x}{\partial x} + V_y\frac{\partial V_x}{\partial y}\right) + \mu\left(\frac{\partial^2 V_x}{\partial x^2} + \frac{\partial^2 V_x}{\partial y^2}\right)$$

For a better estimation of the suction force, the pressure gradient is averaged along the control volumes, which include the central inflow centerline represented in Fig. 2. In Fig. 6, a typical relationship between the pressure gradient and the induced flow field are plotted; two distinct suction flow trends are observed. At the far field of the mouth aperture, the pressure gradient and the spatial velocity are correlated, indicating a substantial suction force for prey recruitment (point C to B). The maximum streamwise velocity is reached at point B, which almost coincides with a local peak of the pressure gradient. Proximal to the mouth aperture and through the deceleration region (point B to A), the pressure gradient drops rapidly, following an oscillatory trend, which could potentially enable prey engulfment. Computational fluid dynamics simulations of adult fish regimes show that the peak flow is located very close to the mouth while our measurements indicate that this is not necessarily true for larval fish. Further experiments are needed to show whether the low-pressure gradient between points B and C is due to some hydrodynamic phenomena specific to larval stages (e.g., the mouth vortex in Figs. 2 and 4 or the low larval tissue compliance of the zebrafish introducing time-delays in the inflow bolus) or whether it is due to the near-wall limitation of our μPIV measurements, which were made closer to the mouth. The near-wall limitation is due to the use of discretized/partial PIV interrogation

windows situated closer to the wall region and is further challenged by the 3D flows that follow the body contour in our application.

3.4 Limitations

In addition to fluid dynamics, the performance of larval fish feeding depends on physiological factors that change constantly as the fish grows, such as optimal ingestion, digestion, and absorption (Rønnestad et al. 2013). The present study focused exclusively on mechanical factors. Furthermore, as this study employed a stationary animal/prey model, which is typical for earlier larval stages, it also ignored the effect of external flow caused by body strike movement (Fuiman and Webb 1988). We captured the feeding cycle in our experiments, but other modes of operation and anatomy may play a role in the resulting flow fields (Gibb 1997). In particular, differentiating the steady-state respiration and feeding cycles was challenging when investigating younger fish. For the larger larvae group (Group 3), it was observed that in addition to normal jaw opening, the respiratory cycle caused ~1 mm/s of peak-induced flow velocity. Respiration-induced flow fields require more detailed studies in the future, though it seems clear that they create significantly lower velocities than those produced during the feeding cycle. In order to compare our results with those from earlier experiments, we tried to capture velocity fields from the side; however, this also proved challenging, since the fish naturally lies on its belly and will often reorient itself. While we obtained good side view vector fields and verified flow both into and out of the fish, these results are not included in this research paper, as they required the use of tricaine (an anesthesia) to capture flat fish orientation under our microscope setup. Finally, our group has recently developed a "true" OCT-PIV technique, which can track the intensities of the particles from the OCT data (Chen et al. 2013; Kowalski et al. 2014). However, the data acquisition rate of this technique only barely satisfies the imaging requirements for capturing the rapid feeding cycles encountered in the present larval stages. Thus, the present study was conducted using the traditional high-speed CMOS cameras.

4 Conclusion

In this study, the induced flow fields present during the suction feeding motions of zebrafish larvae together with the associated jaw movements are analyzed using high-speed μPIV and OCT, respectively. The quantitative results obtained can impact biological studies that focus on inactive predator–prey interactions as well as on the evolution of the complex jaw protrusion mechanisms of bony fishes. The peak velocity of induced flows can soar to 8 mm/s for rapid capture when prey is nearby during a predatory strike from late-stage zebrafish larvae ($L = 20$ mm). Our results enhance the understanding of suction performance from kinematic and morphological perspectives. For the first time in the literature, the present experiments provide the baseline flow regime and the complete external flow fields of a common transgenic animal model at the creeping flow regime.

Acknowledgments We acknowledge Prof. Beth Roman from the University of Pittsburgh for guiding our in-house zebrafish larvae culture and their handling protocols. K.P. was supported by NSF CAREER Award 0954465. R.H. was supported by Israel Science Foundation Grants 158/11 and 695/15.

References

Chen CA, Pekkan K (2013) High-speed three-dimensional characterization of fluid flows induced by micro-objects in deep microchannels. BioChip J 7:95–103

Chen CY, Menon PG, Kowalski W, Pekkan K (2013) Time-resolved OCT-μPIV: a new microscopic PIV technique for noninvasive depth-resolved pulsatile flow profile acquisition. Exp Fluids 54:1–9

China V, Holzman R (2014) Hydrodynamic starvation in first-feeding larval fishes. Proc Natl Acad Sci 111:8083–8088

Dabiri JO, Bose S, Gemmell BJ, Colin SP, Costello JH (2014) An algorithm to estimate unsteady and quasi-steady pressure fields from velocity field measurements. J Exp Biol 217:331–336

Day SW, Higham TE, Cheer AY, Wainwright PC (2005) Spatial and temporal patterns of water flow generated by suction-feeding bluegill sunfish *Lepomis macrochirus* resolved by Particle Image Velocimetry. J Exp Biol 208:2661–2671

Day SW, Higham TE, Wainwright PC (2007) Time resolved measurements of the flow generated by suction feeding fish. Exp Fluids 43:713–724

Day SW, Higham TE, Holzman R, Van Wassenbergh S (2015) Morphology, kinematics, and dynamics: the mechanics of suction feeding in fishes. Integr Comp Biol 55:21–35

Fuiman LA, Webb PA (1988) Ontogeny of routine swimming activity and performance in zebra danios (Teleostei: Cyprinidae). Anim Behav 36:250–261

Gemmell BJ, Adhikari D, Longmire EK (2014) Volumetric quantification of fluid flow reveals fish's use of hydrodynamic stealth to capture evasive prey. J R Soc Interface 11:20130880

Gibb AC (1997) Do flatfish feed like other fishes? A comparative study of percomorph prey-capture kinematics. J Exp Biol 200:2841–2859

Hernandez LU (2000) Intraspecific scaling of feeding mechanics in an ontogenic series of zebrafish, *Danio rerio*. J Exp Biol 203:3033–3043

Higham TE, Day SW, Wainwright PC (2006) Multidimensional analysis of suction feeding performance in fishes: fluid speed, acceleration, strike accuracy and the ingested volume of water. J Exp Biol 209:2713–2725

Holzman R, Collar DC, Day SW, Bishop KL, Wainwright PC (2008) Scaling of suction-induced flows in bluegill: morphological and kinematic predictors for the ontogeny of feeding performance. J Exp Biol 211:2658–2668

Holzman R, China V, Yaniv S, Zilka M (2015) Hydrodynamic constraints of suction feeding in low Reynolds numbers, and the critical period of larval fishes. Integr Comp Biol 55:48–61

Kowalski WJ, Teslovich NC, Menon PG, Tinney JP, Keller BB, Pekkan K (2014) Left atrial ligation alters intracardiac flow patterns and the biomechanical landscape in the chick embryo. Dev Dyn 243:652–662

Parra G, Yúfera M (2000) Feeding, physiology and growth responses in first-feeding gilthead seabream (*Sparus aurata* L.) larvae in relation to prey density. J Exp Mar Biol Ecol 243:1–15

Rønnestad I, Yúfera M, Ueberschär B, Ribeiro R, Saele O, Boglione C (2013) Feeding behaviour and digestive physiology in larval fish: current knowledge, and gaps and bottlenecks in research. Rev Aquac 5:S59–S98

Staab KL, Holzman R, Hernandez LP, Wainwright PC (2012) Independently evolved upper jaw protrusion mechanisms show convergent hydrodynamic function in teleost fishes. J Exp Biol 215:1456–1463

Yaniv S, Elad D, Holzman R (2014) Suction-feeding across fish life stages: flow dynamics from larvae to adults and implications for prey capture. J Exp Biol 217:3748–3757